

Electronic structure and phase transition engineering in NbS_2: Crucial role of van der Waals interactions

Wei Wang(王威), Wen Lei(雷文), Xiaojun Zheng(郑晓军), Huan Li(黎欢), Xin Tang(唐鑫), Xing Ming(明星)
Citation: Chin. Phys. B . 2020, 29(5): 056201 . **doi:** 10.1088/1674-1056/ab8214
Journal homepage: http://cpb.iphy.ac.cn; http://iopscience.iop.org/cpb

What follows is a list of articles you may be interested in

Structural and electrical transport properties of Dirac-like semimetal $PdSn_4$ under high pressure

Bowen Zhang(张博文), Chao An(安超), Yonghui Zhou(周永惠), Xuliang Chen(陈绪亮), Ying Zhou(周颖), Chunhua Chen(陈春华), Yifang Yuan(袁亦方), Zhaorong Yang(杨昭荣)
Chin. Phys. B . 2019, 28(12): 126202 . **doi:** 10.1088/1674-1056/ab50b3

High-pressure electrides: From design to synthesis

Biao Wan(万彪), Jingwu Zhang(张静武), Lailei Wu(吴来磊), Huiyang Gou(缑慧阳)
Chin. Phys. B . 2019, 28(10): 106201 . **doi:** 10.1088/1674-1056/ab3f95

Phase transitions in bismuth under rapid compression

Dong-Liang Yang(杨栋亮), Jing Liu(刘景), Chuan-Long Lin(林传龙), Qiu-Min Jing(敬秋民), Yi Zhang(张毅), Yu Gong(宫宇), Yan-Chun Li(李延春), Xiao-Dong Li(李晓东)
Chin. Phys. B . 2019, 28(3): 036201 . **doi:** 10.1088/1674-1056/28/3/036201

Pressure-induced enhancement of optoelectronic properties in PtS_2

Yi-Fang Yuan(袁亦方), Zhi-Tao Zhang(张志涛), Wei-Ke Wang(王伟科), Yong-Hui Zhou(周永惠), Xu-Liang Chen(陈绪亮), Chao An(安超), Ran-Ran Zhang(张冉冉), Ying Zhou(周颖), Chuan-Chuan Gu(顾川川), Liang Li(李亮), Xin-Jian Li(李新建), Zhao-Rong Yang(杨昭荣)
Chin. Phys. B . 2018, 27(6): 066201 . **doi:** 10.1088/1674-1056/27/6/066201

Exploring the compression behavior of HP-$BiNbO_4$ under high pressure

Yin-Juan Liu(刘银娟), Jia-Wei Zhang(张佳威), Duan-Wei He(贺端威), Chao Xu(许超), Qi-Wei Hu(胡启威), Lei Qi(戚磊), A-Kun Liang(梁阿坤)
Chin. Phys. B . 2017, 26(11): 116202 . **doi:** 10.1088/1674-1056/26/11/116202

Electronic structure and phase transition engineering in NbS_2: Crucial role of van der Waals interactions*

Wei Wang(王威)[1], Wen Lei(雷文)[1], Xiaojun Zheng(郑晓军)[1], Huan Li(黎欢)[1], Xin Tang(唐鑫)[2], and Xing Ming(明星)[1,†]

[1] College of Science, Guilin University of Technology, Guilin 541004, China

[2] Key Laboratory of New Processing Technology for Nonferrous Metal & Materials, Ministry of Education, School of Materials Science and Engineering, Guilin University of Technology, Guilin 541004, China

(Received 6 February 2020; revised manuscript received 13 March 2020; accepted manuscript online 23 March 2020)

Based on first-principles simulations, we revisit the crystal structures, electronic structures, and structural stability of the layered transition metal dichalcogenides (TMDCs) NbS_2, and shed more light on the crucial roles of the van der Waals (vdW) interactions. Theoretically calculated results imply that the vdW corrections are important to reproduce the layered crystal structure, which is significant to correctly describe the electronic structure of NbS_2. More interestingly, under hydrostatic pressure or tensile strain in *ab* plane, an isostructural phase transition from two-dimensional layered structure to three-dimensional bulk in the $I4/mmm$ phase has been uncovered. The abnormal structural transition is closely related to the electronic structure instability and interlayer bonding effects. The interlayer Nb–S distances collapse and the interlayer vdW interactions disappear, concomitant with new covalent bond emerging and increasing coordination number. Present work highlights the significance of the vdW interactions, and provides new insights on the unconventional structural transitions in NbS_2, which will attract wide audience working in the hectic field of TMDCs.

Keywords: NbS_2, high pressure, phase transition, van der Waals (vdW) interactions

PACS: 62.50.–p, 71.20.–b, 71.15.Mb **DOI:** 10.1088/1674-1056/ab8214

1. Introduction

Layered transition metal dichalcogenides (TMDCs) have attracted extensive interests and been intensively studied in recent years.[1] Many monolayer TMDCs have been chemical synthesized or mechanically exfoliated successfully from their bulk phases. Crystal structures and electronic properties of TMDCs can be tuned in a wide range by doping, defect structure, adsorption, strain, or stress. Monolayer and few-layered TMDCs show promising properties and performances, and are widely used in catalysis, sensing, optoelectronics, nanoelectronic and optical devices.[2–8]

In addition to widespread interests in the TMDCs for their promising applications, niobium dichalcogenides NbX_2 (X = S, Se, Te) have been widely studied for a long time because of their superconducting behavior and charge density wave (CDW) order.[9–11] The 2H-NbS_2 is isoelectronic and isostructural with 2H-$NbSe_2$, showing similar superconducting transition temperature. The CDW instability in $NbSe_2$ and its possible interaction with superconductivity have been intensive investigated. However, the research progress of CDW in 2H-NbS_2 is stagnant, which has been attributed to the anharmonic suppression.[12] The nature of the superconducting gap and the pairing mechanism in 2H-NbS_2 are elucidated by *ab initio* anisotropic Migdal–Eliashberg theory, and the system is proposed to be on the verge of a latent CDW instability.[13] With the advent of two-dimensional (2D) materials, synthesis of ultrathin, large-size monolayer and few-layered NbS_2 becomes more and more mature.[14–17] Recently, an enhanced tendency toward CDW order in the 2D limit is observed in NbS_2.[18–21]

The crystal structure, topological state, and transport properties of the layered materials can be tuned by strain, stress, and pressure, resulting in interesting phenomena and properties such as topological transition,[22] metal–insulator transition,[23–25] and ferroelastic phase transition.[26] As shown in Fig. 1, three polytypes of NbS_2 have been successfully synthesized and feature with one-layer trigonal (1T), two-layer hexagonal (2H), and three-layer rhombohedral (3R) structures.[27–31] High-pressure experimental investigations indicate that the structure of 3R-NbS_2 is highly anisotropic under compression,[32,33] and the superconducting transition temperature and upper critical field of 2H-NbS_2 increase simultaneously along with the increasing pressure.[34] Density functional theory (DFT) calculations predict that a tensile strain can switch the magnetic states in monolayer $NbSe_2$ and NbS_2.[35,36] In addition, the structural phase transition and superconducting properties of NbS_2 under high pressure have been studied recently by first-principles calculations, where the 2H phase transforms to a new tetragonal $I4/mmm$ structure at 26 GPa.[37] The $I4/mmm$ phase [Fig. 1(d)] is predicted to be mechanically and dynamically stable at high pres-

*Project supported by the National Natural Science Foundation of China (Grant No. 11864008) and Guangxi Natural Science Foundation, China (Grant Nos. 2018GXNSFAA138185 and 2018AD19200). High performance computational resources provided by LvLiang Cloud Computing Center of China and National Supercomputer Center on TianHe-2 are gratefully acknowledged.

†Corresponding author. E-mail: mingxing@glut.edu.cn

© 2020 Chinese Physical Society and IOP Publishing Ltd

sure by calculating the elastic constants and phonon dispersion, and exhibits a higher superconducting temperature than the 2H phase. Singh *et al.* discovered an increasing number of conduction bands crossing the Fermi level and higher conductivity in 2H-NbS_2 by applying uniaxial strain along the *c*-axis.[38] As shown in Fig. 1, these experimentally already-synthesized phases (1T, 2H, and 3R structures) and theoretically predicted $I4/mmm$ phase crystallize in layered structure. Similar to other layered TMDCs materials, the weak interlayer van der Waals (vdW) interactions should play a crucial role in bonding together the 2D layers in the bulk. Obviously, it is unreasonable to ignore the interlayer vdW interactions in previous theoretical studies on NbS_2 to explore the structural transitions and electronic structures under high pressure or strain.[37,38]

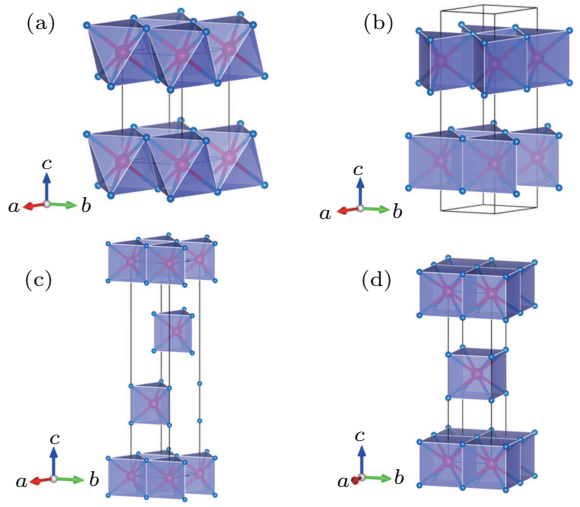


Fig. 1. The crystal structures of NbS_2 with space group (a) $P\bar{3}m1$ (1T), (b) $P6_3/mmc$ (2H), (c) $R3m$ (3R), and (d) $I4/mmm$. Big (red) and small (blue) balls represent Nb and S atoms, respectively. The solid line denotes the unit cell. The polyhedra highlight the coordination environments of the Nb ions.

In the present study, we want to revisit the crystal structure and electronic structure of NbS_2 and probe the structural stability of bulk NbS_2 under high pressure by first-principles simulation including vdW corrections. Theoretically calculated results are consistent with the available experimental results of the 2H and 3R phases of NbS_2, indicating that the vdW corrections indeed play a crucial role in the layered crystallographic structures, and improve the description of the electronic states around the Fermi level. Furthermore, we discover that the lattice parameters of the $I4/mmm$ phase remarkably change at 32 GPa, accompanied with abrupt shortening of the interlayer distances and increasing coordination number. The structural transition from layered structure to three-dimensional (3D) bulk in $I4/mmm$ phase can be achieved by imposing a tensile strain in *ab*-plane, which is originated from the interlayer bonding effects. Our reported results are expected to attract extensive interests from both of the theoretical and experimental communities in the hectic field of TMDCs.

2. Computational and analytical methods

We performed the calculations within the framework of DFT with the projector augmented wave (PAW) method[39,40] implemented in the Vienna *ab initio* simulation package (VASP) code.[41] Generalized gradient approximation (GGA) with the Perdew–Burke–Ernzerhof (PBE) parameterization was used for the exchange–correlation potential.[42] For geometry optimization and electronic properties calculations, the optimized exchange vdW functional (opt-B88-vdW)[43] was applied to take into account the vdW interactions. The kinetic-energy cutoff was set up to 520 eV. In order to ensure the accuracy of the structural optimization and allow the atoms to move smoothly, the symmetries were canceled during the relaxing process. Owing to the presence of heavy 4d-electrons in Nb, spin–orbit coupling (SOC) was turned on when calculating the electronic properties. We first confirmed the credibility of the calculations by optimizing the crystal structures of the experimentally already-synthesized phases (1T, 2H, and 3R structures) at ambient condition (0 GPa), then gradually increased the hydrostatic pressure from 0 GPa to 50 GPa with an interval of 5 GPa to simulate the structural responses under compression. The *k*-points distance was fixed to 0.2 $Å^{-1}$ in the reciprocal space. The accuracies of the target pressure and energy convergence for all structure optimizations were better than 0.005 GPa and 10^{-6} eV, respectively.

3. Results and discussion

In order to examine the influences of the vdW interactions, the crystal structures of the experimentally already-synthesized phases (1T, 2H, and 3R structures) are first optimized at ambient condition (0 GPa) with several vdW-corrected functionals.

Table 1. Comparison of experimental data with theoretically calculated lattice constants *a*, *c* and unit cell volume *V* for the experimentally already-synthesized NbS_2 (1T, 2H, and 3R structures) at ambient condition.

Structure	Reference	*a*/Å	*c*/Å	*c*/*a*	*V*/Å^3
1 T	Exp.[27]	3.420	5.938	1.736	60.16
	Theo.[37]	3.253	5.341	1.642	48.95
	This work	3.384	5.944	1.757	58.96
2H	Exp.[12]	3.330	11.950	3.589	114.76
	Exp.[27]	3.418	11.860	3.470	119.99
	Exp.[28]	3.310	11.890	3.592	112.82
	Theo.[37]	3.287	11.421	3.475	106.86
	Theo.[44]	3.332	12.106	3.633	116.39
	Theo.[44]	3.313	12.074	3.644	114.76
	This work	3.358	12.049	3.588	117.66
3R	Exp.[28]	3.330	17.810	5.348	171.03
	Exp.[29]	3.335	17.834	5.348	171.78
	Exp.[30]	3.330	17.918	5.381	172.07
	Theo.[37]	3.286	17.577	5.349	164.37
	This work	3.357	18.357	5.468	179.10

As shown in Table 1, the lattice constants obtained by the opt-B88-vdW correction method[43] agree better with the

experimental data[12,27–30] than the previous reported theoretical results calculated by local density approximate (LDA) method.[37] We note that although employed the same GGA-PBE functional, even PBE hybrid functional (PBE0),[44] the calculated unit cell parameters obtained in the present work are closer to the experiment data, implying that the vdW corrections are indeed very important to describe the layered structure of the NbS_2 material. Therefore, the vdW interactions undoubtedly should be taken into account to simulate the structural transitions under high pressure.

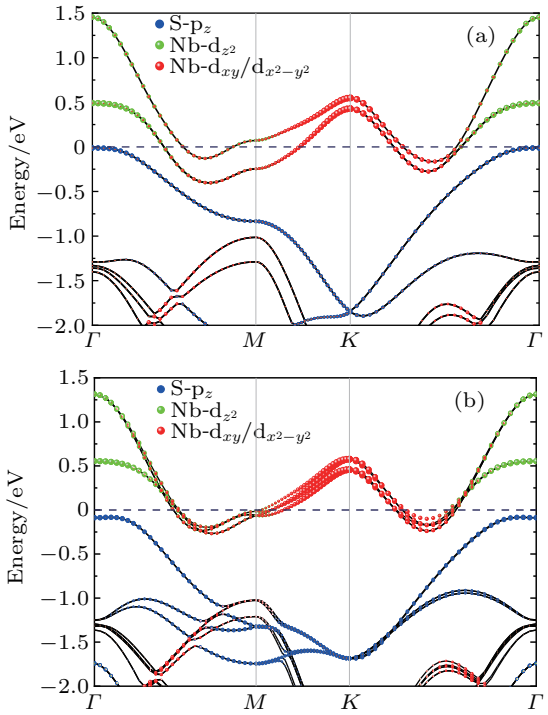


Fig. 2. Calculated band structures (solid black lines) and the projection of the electronic states on the level of GGA with opt-B88-vdW correction for the two common polytypes of NbS_2: (a) 2H and (b) 3R phases. The orbital contributions are proportional to the sizes of the colored balls, as indicated in the legend: S p_z (blue), Nb d_{z^2} (green), and Nb $d_{xy}/d_{x^2-y^2}$ (red).

Based on the optimized structures, the GGA with opt-B88-vdW correction method is further verified by calculating the band structures of the two common polytypes of NbS_2 (2H and 3R phases). As shown in Fig. 2, the electronic states around the Fermi level for 2H-NbS_2 phase are in good agreement with the electronic structure calculated within GW many-body interaction corrections, where the S p_z and Nb d_{z^2} states are pushed apart at the Γ point.[45] In contrast to the three bands crossing the Fermi level calculated by LDA or PBE,[13,44,45] there are only two bands crossing the Fermi level at Γ and K points [Fig. 2(a)], emerging from the bilayer splitting of the Nd d bands. The band structures crossing the Fermi level coincide with the experimental energy and momentum distribution curves.[46] Especially, the GW calculation results need a rigid shift of the Fermi level to bring in excellent agreement with the experiments.[45] The present calculations find that the hole pockets centered at Γ (K) predominantly arise from Nb d_{z^2} ($d_{xy}/d_{x^2-y^2}$), and the band dispersions along the Γ–K direction are consistent well with the angle-resolved photoemission spectroscopy (ARPES) experimental results of 2H-NbS_2.[46] In addition, the obtained band structure of 3R-NbS_2 successfully reproduces the previous theoretical results using various exchange–correlation functionals.[47,48] The electronic states around Fermi level show similar dispersion characteristics and compositions to those of the 2H phase, arising from two and three repeat trigonal prismatic layers for 2H and 3R NbS_2 [Figs. 1(b) and 1(c)], respectively. SOC only has minor impact on the electronic structures, except that it leads to band splitting around the K point.[45,48] The present theoretically calculated results indicate that the vdW corrections really play a critical role in bonding together the layered structures. Furthermore, the vdW functional improves the description of the electronic structure through their effects on the crystal structure, giving better agreement with the available experimental results of the 2H and 3R phases of NbS_2.[49]

Figure 3 presents the volume evolutions with compression, which are fitted by the Birch–Murnaghan isothermal equation of state (BM-EOS).[50] The fitted equilibrium volumes (V_0) are consistent well with the optimized results and experimental data at ambient condition (Table 1). Attributed to the similar layered structure of the experimentally already-synthesized structures (1T, 2H, and 3R phases), their bulk moduli (B_0), the pressure derivative of the bulk modulus (B_0'), and volumes at zero pressure (V_0) are close to each other. The theoretically calculated bulk modulus (54 GPa) coincides well with the experimentally derived value (57 GPa) of the 3R phase.[32] A notable feature is that the volume of the $I4/mmm$ phase shows an abnormal change between 31 GPa and 32 GPa, which is assigned to the transition from the low pressure (LP) to high pressure (HP) phase [Fig. 3(d)]. The bulk modulus of the $I4/mmm$ phase increases from 47.66 GPa to 135.07 GPa from LP to HP range. The HP $I4/mmm$ phase is harder to be compressed than the other three layered phases (1T, 2H, and 3R phases) at ambient condition, which agrees well with the 3D structural characteristics of the HP $I4/mmm$ phase [inset in Fig. 6(d)] with respect to the 2D layered structures of the 1T, 2H, and 3R phases (Fig. 1).

The energetic mechanism and kinetic mechanism are key factors to determine whether a phase can stably exist or undergo a transition under pressure.[51–53] In order to explore the structure stability of NbS_2 under high pressure, we plot the enthalpy difference (ΔH) for these experimentally already-synthesized structures (1T, 2H, and 3R phases) relative to the theoretically predicted $I4/mmm$ phase in Fig. 4 with vdW interaction of opt-B88. The previous studies on TiO_2 polymorphs indicate that the vdW interaction is an indispensable

factor for describing the exact energy and enthalpy under pressure, so that the accurate phase transitions can be captured in accordance with the experiments.[54] At ambient pressure condition (0 GPa), the enthalpy of the 2H phase is comparable to that of the 3R phase, which is lower than the 1T one. The theoretically calculated results are in line with the fact that the 1T phase is hard to be synthesized in bulk, only reported in thin film[27] or monolayer forms.[55] In contrast, the 2H and 3R phases are two common polymorphs been successfully synthesized in bulk forms.[28,31]

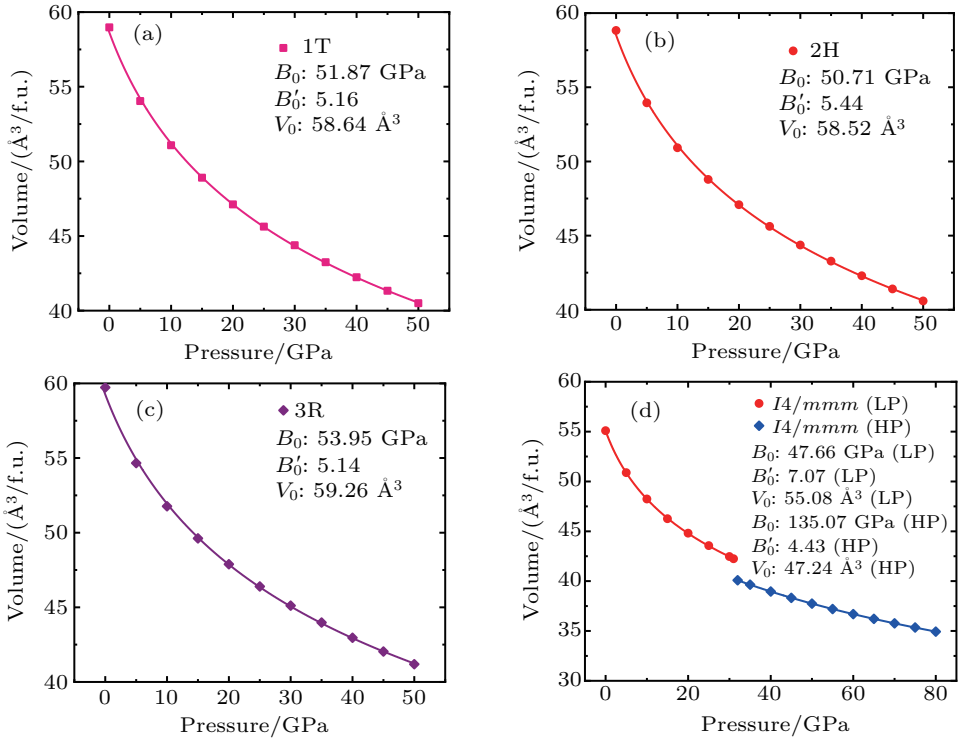


Fig. 3. Unit cell volume variations with the increasing pressure for (a) 1T, (b) 2H, (c) 3R, and (d) $I4/mmm$ phases. The solid lines are fitted by BM-EOS.

In addition, the enthalpy of the $I4/mmm$ phase is far higher than those of the three experimental phases (1T, 2H, and 3R) at ambient pressure. These tendencies are consistent well with the previous reported theoretical results.[37] As shown in Fig. 1, although the Nb atoms are six-coordinated with S atoms in all three experimental phases, the coordination polyhedra around the Nb atoms are different. The 1T phase contains hexagonal tightly packed S atoms and edge-sharing NbS_6 octahedra [Fig. 1(a)].[27] Both the double-layer 2H and triple-layer 3R structures are consisted of trigonal prisms with different interlayer relative positions of the polyhedra [Figs. 1(b) and 1(c)], whereas the $I4/mmm$ phase is a layered structure with face-sharing eight-coordinated body-center-cubic polyhedra [Fig. 1(d)]. When the pressure increases to 17 GPa, the six-coordinated 3R phase transforms to the 1T phase with the coordination polyhedra changing from triangular prisms to octahedra, but the coordination number keeps unchanged. Under further compression, a transition from 1T phase to $I4/mmm$ phase takes place at 35 GPa, accompanying with a volume collapse of 8.1% [Fig. 5(a)]. Consistent with the previous experimental results that the 2H phase is stable up to 20 GPa,[34] the 2H phase maintains thermodynamic stability up to 38 GPa under compression and then transforms to the $I4/mmm$ phase, accompanying with a volume collapse of 7.8% [Fig. 5(b)]. The volume evolutions show discontinuous changes at the transition pressures, suggesting that the structural transitions are first order. It should be noted that the transition pressures in the present work differ from the previous theoretical results obtained by Liu *et al.*[37] The differences mainly come from the choice of the exchange–correlation parameters (GGA vs. LDA) and the vdW corrections included during the geometrical optimization.

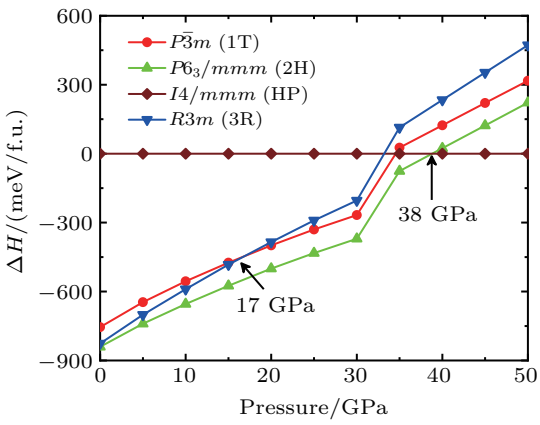


Fig. 4. Calculated enthalpy differences (ΔH) of the experimentally synthesized phases (1T, 2H, and 3R) relative to the theoretically predicted $I4/mmm$ phase under hydrostatic pressure.

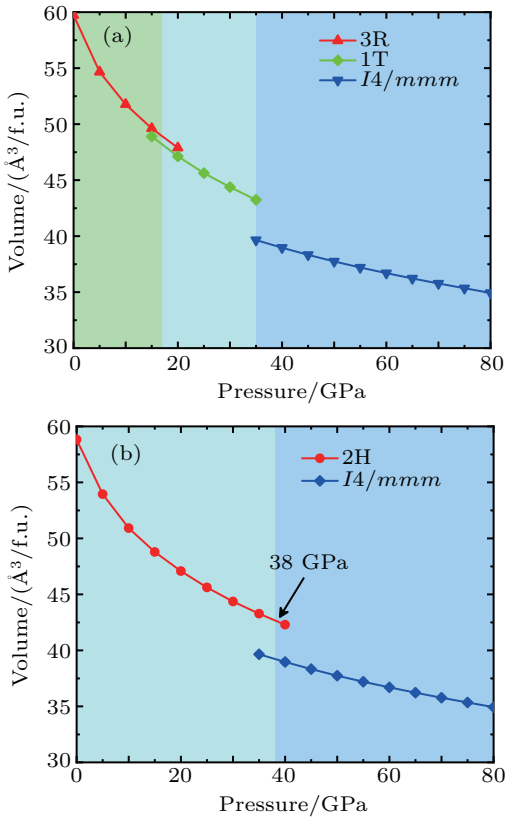


Fig. 5. Variations of the volume as a function of pressure. (a) Structural phase transitions from 3R to 1T phase at 17 GPa, and from 1T to $I4/mmm$ phase at 35 GPa. (b) Structural phase transition from 2H to $I4/mmm$ phase at 38 GPa.

Another noteworthy point is that the slopes of the enthalpy increase significantly around the pressure range of 30–35 GPa (Fig. 4). In order to inspect the detail of the abnormal change of the enthalpy and the lattice volume variation of the $I4/mmm$ phase, we decrease the pressure step to 1 GPa in the range of 30–35 GPa, and increase the pressure range up to 80 GPa [Fig. 3(d)]. Both the enthalpy and energy show abnormal changes between 31 GPa and 32 GPa [Figs. 6(a) and 6(b)]. The volume collapse causes a slight decrease of enthalpy and an abnormal increase of energy at 32 GPa. Similar to the cases of the 2H and 3R phases, the compression behavior of the $I4/mmm$ phase shows strong anisotropy.[32–34] The lattice constant c obviously decreases with increasing compression, whereas lattice constant a is almost unchanged. The compressibility is consistent with the layered structure stacking along the crystallographic c axis, arising from the weak interlayer vdW interactions. Along with the pressure increasing up to 32 GPa, the lattice constants show discontinuous changes, but the crystal symmetry and the space group are maintained. As shown in Fig. 6(c), the lattice constant a expands a bit and c shrinks a lot at 32 GPa; the lattice constants are $a = b = 3.01$ Å, $c = 9.35$ Å at 31 GPa and $a = b = 3.17$ Å, $c = 7.99$ Å at 32 GPa. The variations of enthalpy, energy, and lattice constants indicate that an isostructural transition occurs in the tetragonal $I4/mmm$ phase.

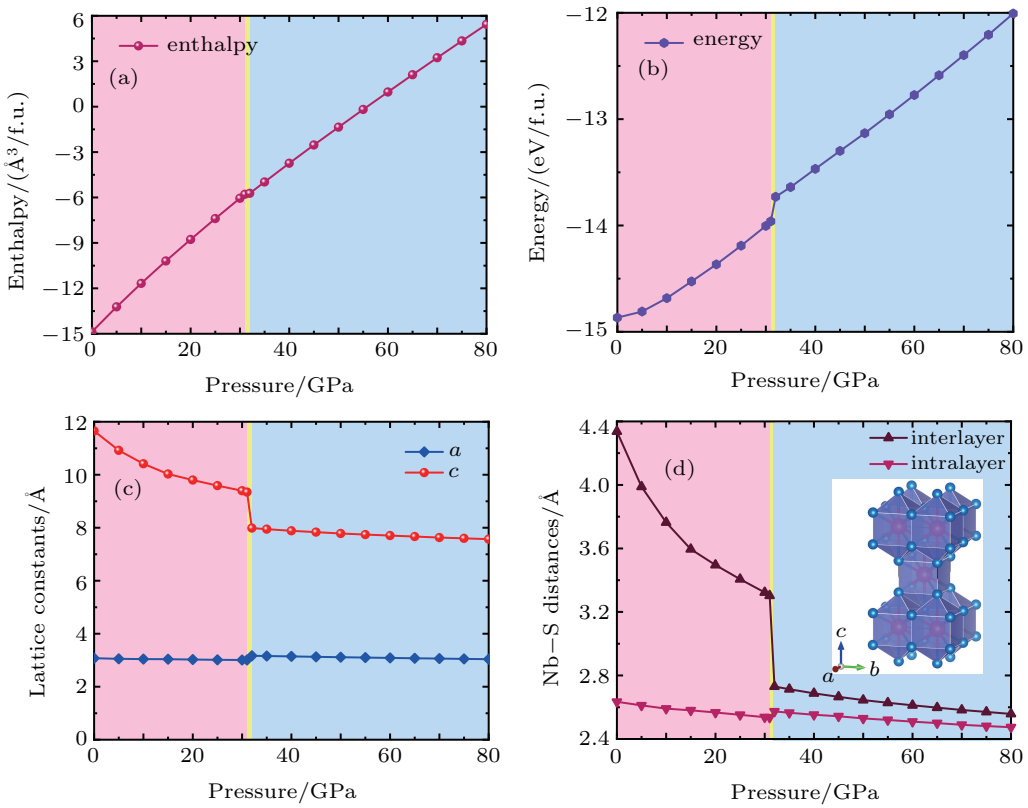


Fig. 6. Variations of the (a) enthalpy, (b) energy, (c) lattice constants, and (d) interlayer and intralayer Nb–S bond lengths as a function of pressure for the $I4/mmm$ phase up to 80 GPa. The inset in (d) shows the structure of HP $I4/mmm$ phase. The transition region is highlighted around 31–32 GPa.

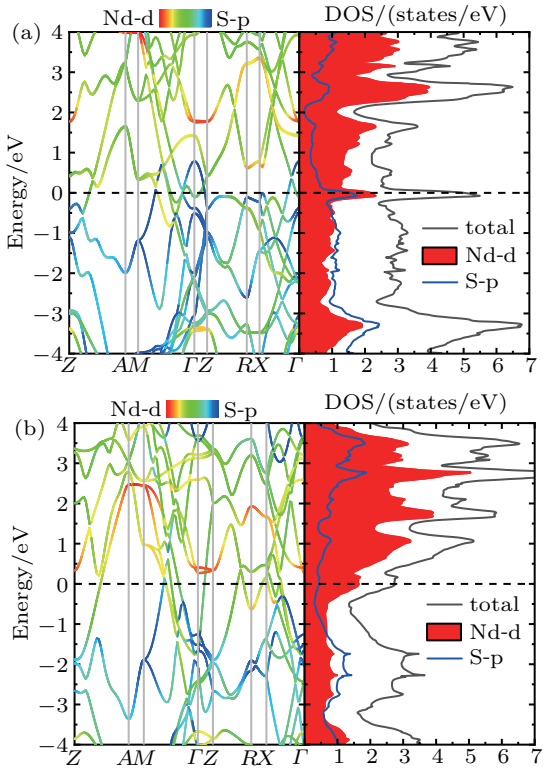


Fig. 7. Electronic band structure and density of states of $I4/mmm$-NbS_2 at (a) 31 GPa and (b) 32 GPa. The colors of the band structure denote the contributions from Nb d (red) and S p (blue) states, and strong hybridizations between them.

In order to get further insights into the structural phase transition in the $I4/mmm$ phase, we calculate the electronic structure of the $I4/mmm$ phase around the pressure range of 31–32 GPa. The band structures and density of states (DOS) are displayed in Fig. 7. As shown in the band structures, both the conduction bands and valence bands overlap with each other near the Fermi level, displaying good metallic properties. The orbital overlap and atomic interaction are enhanced greatly under the compression. As shown in Fig. 7(a), the bands near the Fermi level show weak dispersion along the Z–R–X–Γ direction, leading to localized electron states with heavy effective mass. By contrast, the bandwidths are obviously broadened along the M–Γ–Z direction, leading to the delocalization of electrons. By further increasing the pressure, the out-of-plane dispersion of the bonding orbitals and antibonding orbitals increases significantly along the Z–A–M direction [Fig. 7(b)]. These changes of the band structures indicate an enhancement of bonding effect, and new bonds emerge in the crystal. As shown in the electronic structures, the Nb d states strongly hybridize with the S p states, and make major contributions to the bands around the Fermi level. Especially, a sharp peak locates close to the Fermi level in the DOS at 31 GPa, consistent with the almost degenerate band lying near the Fermi level along the Z–R direction [Fig. 7(a)]. The close proximity of this DOS peak to the Fermi level favors an electronic instability at 31 GPa.[56] With further compression, a phase transition will take place to eliminate the instability. The sharp peak indeed disappears and the DOS at the Fermi level reduces at 32 GPa [Fig. 7(b)]. The electronic instability is close related to the interlayer vdW interactions. The interlayer Nb–S distance is 3.30 Å at 31 GPa [Fig. 6(d)], indicating that the interlayer vdW interaction is at the edge of existence (3.1-5.0 nm), causing an instability of electronic state. Further compression reduces the interlayer Nb–S distance to 2.75 Å at 32 GPa. Consequently, the interlayer distance is below the threshold of vdW interactions, which leads to that the interlayer vdW forces weaken and the electronic structure transforms to a new stable state.

The origin of the transition around 31 GPa can be further explored by the electron localization function (ELF).[57] The ELF is a function ranging from 0 to 1, indicating the type and strength of the bonding. As shown in Fig. 8, the ELF is close to 0.9 around the S atoms, indicating that polar bonds exist. Electrons are transferred from Nb to S and molecular orbitals are formed. It is clearly seen that a layered structure exists at 31 GPa with eight-fold coordinated Nb [Fig. 8(a)]. However, the layered structure has become blurred at 32 GPa [Fig. 8(b)]. The vdW radii of Nb and S ions are 2.15 Å and 1.8 Å, whereas the covalent radii of Nb and S ions are 1.64 Å and 1.05 Å, respectively.[58,59] The interlayer and intralayer Nb–S distances are 3.301 Å and 2.536 Å at 31 GPa, and 2.731 Å and 2.574 Å at 32 GPa, respectively [Fig. 6(c)]. Apparently, the interlayer Nb–S distance has reached the requirement of bonding at 32 GPa. New interlayer Nb–S bonds formation leads to the coordination number of Nb increasing from eight to ten, and the interlayer vdW interaction no longer plays the dominant role, but is replaced by a negligible weak interaction described by standard GGA.[60] Accordingly, the $I4/mmm$ structure transforms from a layered phase to 3D bulk phase due to the interlayer bonding effects, resulting in a higher compactness and lesser compressibility for the $I4/mmm$ HP structure as shown in Fig. 6(d). Pressure-induced decrease or increase of the inter-atom distance usually causes variations of the coordination number. Similar phenomenon has been reported in Bi_2Te_3 layered structure, where the pressure breaks the layered structure with coordination number increasing from six to eight.[61]

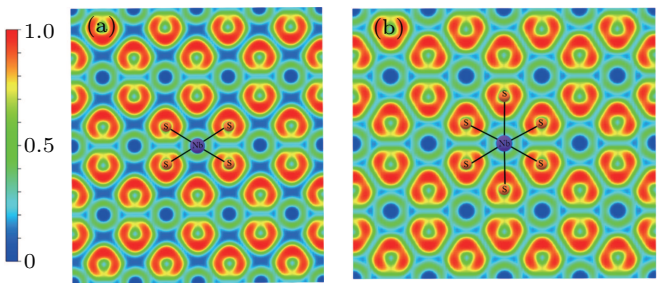


Fig. 8. ELF projected on the (110) crystalline plane for the $I4/mmm$ phase at (a) 31 GPa and (b) 32 GPa. The scale of ELF is ranging from 0 (blue) to 1 (red) and the interval is 0.1.

We further examine the structural stability of the $I4/mmm$ phase under tensile strain in *ab*-plane. Accompanied with the in-plane stretching, the lattice constant c and the interlayer Nb–S distances are gradually compressed. As shown in Fig. 9, the lattice constants c, c/a ratio, and interlayer Nb–S distances show discontinuous changes with the tensile strain increasing from 8% to 9%. The energy evolution also shows different variation tendency around this strain range. With the tensile strain increasing up to 8%, the interlayer Nb–S distances gradually shrink from 4.337 Å to 3.696 Å. The lattice constant c compression accompanied with the *ab*-plane stretching renders the interlayer Nb–S distances on the verge of the vdW interactions. Further increasing the tensile strain, the interlayer Nb–S distances collapse and the interlayer vdW interactions disappear, concomitant with new covalent bond emerging and structure transforming from layered 2D to 3D bulk. The calculated electronic structures show similar character with the cases under high pressure, indicates that an instable electronic state becomes stable under compression. The interlayer bonding of Nb and S triggers the structural transition from 2D layered structure to 3D bulk phase. We can expect the structural transition tuned by the tensile strain to be realized in epitaxial films on appropriate substrates.

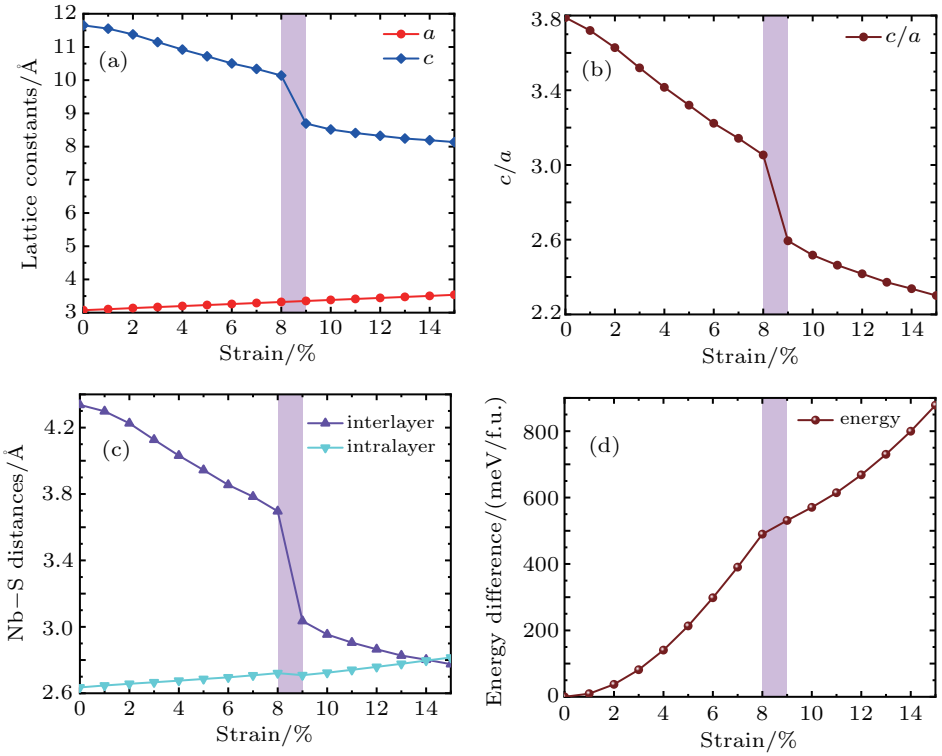


Fig. 9. Variations of the (a) lattice parameters, (b) c/a ratio, (c) inter-atomic distances, and (d) energy under tensile strains in *ab*-plane of the $I4/mmm$ phase.

4. Conclusion

In summary, the stabilities of NbS_2 under hydrostatic pressure have been investigated systematically based on DFT calculations with the inclusion of vdW corrections. We not only confirm the previous theoretically predicted structural transition, but also present electronic structures in better agreement with the available experimental results of the experimentally already-synthesized bulk phases. Furthermore, the structural transition from 2D layered structure to 3D bulk phase in the tetragonal $I4/mmm$ phase is explored at 32 GPa, which can be achieved under tensile strain in *ab*-plane. The unusual structural transformation and electronic structure variation interplay with the change of interlayer bonding. The present work not only highlights the vdW interactions in forming the layered crystal structure, but also implies the critical role played by the vdW interactions in the structural transition of NbS_2. We provide new insights into the description of the structural stability of NbS_2 and complement the content of phase transition engineering.

References

[1] Manzeli S, Ovchinnikov D, Pasquier D, Yazyev O V and Kis A 2017 *Nat. Rev. Mater.* **2** 17033
[2] Chhowalla M, Shin H S, Eda G, Li L J, Loh K P and Zhang H 2013 *Nat. Chem.* **5** 263
[3] Ma X, Zhang R, An C, Wu S, Hu X and Liu J 2019 *Chin. Phys. B* **28** 037803
[4] Liu T, Tong L, Huang X and Ye L 2019 *Chin. Phys. B* **28** 017302
[5] Guan Z, Ni S and Hu S 2018 *J. Phys. Chem. C* **122** 6209
[6] Shu H, Wang Y and Sun M 2019 *Phys. Chem. Chem. Phys.* **21** 15760
[7] Cui Z, Ren K, Zhao Y, Wang X, Shu H, Yu J and Sun M 2019 *Appl. Surf. Sci.* **492** 513
[8] Guan Z, Lian C S, Hu S, Ni S, Li J and Duan W 2017 *J. Phys. Chem. C* **121** 3654

[9] Wilson J A, Di Salvo F J and Mahajan S 1975 *Adv. Phys.* **24** 117
[10] Wilson J A, Di Salvo F J and Mahajan S 1974 *Phys. Rev. Lett.* **32** 882
[11] Neto and A H Castro 2001 *Phys. Rev. Lett.* **86** 4382
[12] Leroux M, Le Tacon M, Calandra M, Cario L, Measson M A, Diener P and Rodiere P 2012 *Phys. Rev. B* **86** 155125
[13] Heil C, Poncé S, Lambert H, Schlipf M, Margine E R and Giustino F 2017 *Phys. Rev. Lett.* **119** 087003
[14] Dash J K, Chen L, Dinolfo P H, Lu T M and Wang G C 2015 *J. Phys. Chem. C* **119** 19763
[15] Zhao S, Hotta T, Koretsune T, Watanabe K, Taniguchi T, Sugawara K and Kitaura R 2016 *2D Mater.* **3** 025027
[16] Wang X, Lin J, Zhu Y, Luo C, Suenaga K, Cai C and Xie L 2017 *Nanoscale* **9** 16607
[17] Kozhakhmetov A, Choudhury T H, Al Balushi Z Y, Chubarov M and Redwing J M 2018 *J. Cryst. Growth* **486** 137
[18] Leroux M, Cario L, Bosak A and Rodiere P 2018 *Phys. Rev. B* **97** 195140
[19] Bianco R, Errea I, Monacelli L, Calandra M and Mauri F 2019 *Nano Lett.* **19** 3098
[20] Güller F, Vildosola V L and Llois A M 2016 *Phys. Rev. B* **93** 094434
[21] Tresca C and Calandra M 2019 *2D Mater.* **6** 035041
[22] Rajaji V, Dutta U, Sreeparvathy P C, Sarma S C, Sorb Y A, Joseph B and Narayana C 2018 *Phys. Rev. B* **97** 085107
[23] Naumov P G, ElGhazali M A, Mirhosseini H, Süß V, Morosan E, Felser C and Medvedev S A 2018 *J. Phys.-Condes. Matter* **30** 035401
[24] Radisavljevic B and Kis A 2013 *Nat. Mater.* **12** 815
[25] Nayak A P, Bhattacharyya S, Zhu J, Liu J, Wu X, Pandey T and Lin J F 2014 *Nat. Commun.* **5** 1
[26] Lei W, Cai B, Zhou H, Heymann G, Tan X, Zhang S and Ming X 2019 *Nanoscale* **11** 12317
[27] Carmalt C J, Manning T D, Parkin I P, Peters E S and Hector A L 2004 *J. Mater. Chem.* **14** 290
[28] Jellinek F, Brauer G and Müller H 1960 *Nature* **185** 376
[29] Ge W, Kawahara K, Tsuji M and Ago H 2013 *Nanoscale* **5** 5773
[30] Morosin B 1974 *Acta. Crystallogr. B* **30** 551
[31] Fisher W G and Sienko M J 1980 *Inorg. Chem.* **19** 39
[32] Ehm L, Knorr K and Depmeier W 2002 *Z. Krist-Cryst. Mater.* **217** 522
[33] Jones Jr R E, Shanks H R, Finnemore D K and Morosin B 1972 *Phys. Rev. B* **6** 835
[34] Tissen V G, Osorio M R, Brison J P, Nemes N M, García-Hernández M, Cario L and Suderow H 2013 *Phys. Rev. B* **87** 134502
[35] Xu Y, Liu X and Guo W 2014 *Nanoscale* **6** 12929
[36] Zhou Y, Wang Z, Yang P, Zu X, Yang L, Sun X and Gao F 2012 *ACS Nano* **6** 9727
[37] Liu Z L, Cai L C and Zhang X L 2014 *J. Alloy. Compd.* **610** 472
[38] Gjerding M, Pandey M and Thygesen K 2017 *Nat. Commun.* **8** 15133
[39] Blöchl P E 1994 *Phys. Rev. B* **50** 17953
[40] Kresse G and Joubert D 1999 *Phys. Rev. B* **59** 1758
[41] Kresse G and Furthmüller J 1996 *Phys. Rev. B* **54** 11169
[42] Perdew J P, Burke K and Ernzerhof M 1996 *Phys. Rev. Lett.* **77** 3865
[43] Klimeš J, Bowler D R and Michaelides A 2010 *J. Phys.-Condens. Matter* **22** 022201
[44] Kuc A, Zibouche N and Heine T 2011 *Phys. Rev. B* **83** 245213
[45] Heil C, Schlipf M and Giustino F 2018 *Phys. Rev. B* **98** 075120
[46] Sirica N, Mo S K, Bondino F, Pis I, Nappini S, Vilmercati P and Vobornik I 2016 *Phys. Rev. B* **94** 075141
[47] Machida T, Kohsaka Y, Iwaya K, Arita R, Hanaguri T, Suzuki R and Iwasa Y 2017 *Phys. Rev. B* **96** 075206
[48] Gjerding M N, Pandey M and Thygesen K S 2017 *Nat. Commun.* **8** 15133
[49] Xiao S L, Yu W Z and Gao S P 2016 *Surf. Sci.* **653** 107
[50] Birch F 1947 *Phys. Rev.* **71** 809
[51] Lei W, Zhang S, Heymann G, Tang X, Wen J, Zheng X and Ming X 2019 *J. Mater. Chem. C* **7** 2096
[52] Zhang S, He J, Zhao Z, Yu D and Tian Y 2019 *Chin. Phys. B* **28** 106104
[53] Wan B, Zhang J, Wu L and Gou H 2019 *Chin. Phys. B* **28** 106201
[54] Zhu T and Gao S P 2014 *J. Phys. Chem. C* **118** 11385
[55] Chen X, Gu Y, Tao G, Pei Y, Wang G and Cui N 2015 *J. Mater. Chem. A* **3** 18898
[56] Zhu J X, Janoschek M, Chaves D S, Cezar J C, Durakiewicz T, Ronning F and Bauer E D 2016 *Phys. Rev. B* **93** 144404
[57] Savin A, Nesper R, Wengert S and Fässler T F 1997 *Angew. Chem. Int. Edit* **36** 1808
[58] Batsanov S 2001 *Inorg. Mater.* **37** 871
[59] Cordero B, Gómez V, Platero-Prats A E, Revés M, Echeverría J, Cremades E and Alvarez S 2008 *Dalton Trans.* **21** 2832
[60] Sun A, Gao S P and Gu G 2019 *Phys. Rev. Mater.* **3** 104604
[61] Zhu L, Wang H, Wang Y, Lv J, Ma Y, Cui Q and Zou G 2011 *Phys. Rev. Lett.* **106** 145501